Journal of Catalysis 277 (2011) 64–71

Contents lists available at ScienceDirect

Journal of Catalysis

journal homepage: www.elsevier.com/locate/jcat

Temperature-induced evolution of reaction sites and mechanisms during preferential oxidation of CO

Richard Kydd [a], Davide Ferri [b,*], Paul Hug [b], Jason Scott [a], Wey Yang Teoh [a,*,1], Rose Amal [a]

[a] ARC Centre of Excellence for Functional Nanomaterials, School of Chemical Engineering, University of New South Wales, Sydney, NSW 2052, Australia
[b] Empa, Swiss Federal Laboratories for Materials Science and Technology, Laboratory for Solid State Chemistry and Catalysis, Ueberlandstrasse 129, CH-8600 Dübendorf, Switzerland

ARTICLE INFO

Article history:
Received 1 May 2010
Revised 25 August 2010
Accepted 14 October 2010

Keywords:
Copper
Ceria
PROX
H_2-TPR
CO-TPR
DRIFTS
Modulation spectroscopy

ABSTRACT

Active sites responsible for the preferential oxidation of carbon monoxide were investigated using 4 wt.% Cu–CeO_2 catalysts prepared by flame spray pyrolysis. Surface redox properties of the catalyst were assessed using a series of temperature-programmed reduction (CO, H_2 and mixed) experiments, as well as *operando* infrared spectroscopy. It was demonstrated that CO and H_2 react at identical surface sites, with CO_2 formation proceeding simultaneously via three distinct Cu^{n+}–CO carbonyl species. The origin of high catalytic selectivity towards CO at below 150 °C stems from the carbonyl stabilization effect on the catalyst surface, preventing adsorption and subsequent oxidation of H_2. Under non-selective conditions at higher temperatures, a gradual red-shift and loss of intensity in the carbonyl peak was observed, indicating reduction of Cu^+ to Cu^0, and the onset of an alternate redox-type oxidation mechanism where CO and H_2 compete for the oxidation sites. These results for Cu–CeO_2 suggest that improved low-temperature catalytic activity will only be achieved at the expense of reduced high-temperature selectivity and vice versa.

1. Introduction

Industrial production of H_2 via the sequential steam reforming and water–gas-shift (WGS) reactions is becoming an inevitable process in line with the implementation of a hydrogen economy. At the core of H_2 energy conversion lies the polymer electrolyte membrane (PEM) fuel cells, which is capable of efficient generation of electricity via the diffusion of protons across an ionic membrane [1]. However, an inherent limitation of PEM fuel cells is poisoning, and deactivation of the Pt anode by CO, where reduction of CO concentration to below 50 ppm (unachievable by WGS) is necessary for prolonged high performance [2]. Hence, an intermediate preferential oxidation of CO (PROX) reaction is necessary to selectively reduce the amount of CO without compromising the amount of H_2. For this reaction, Cu–CeO_2 is a promising candidate as it displays high levels of performance and stability [3], while being orders of magnitude cheaper than conventional precious metal alternatives (e.g. Pt, Au and Pd).

Catalytic performance of Cu–CeO_2 has been typified by high levels of activity and selectivity at low temperatures (<120 °C) and gradual losses in selectivity at higher temperatures [4–8]. Kinetic studies have prompted earlier reports of a redox-type mechanism [8], in which lattice oxygen from the catalyst surface is removed by the CO (or H_2), forming a surface oxygen vacancy in the process. Completion of the catalytic cycle was then proposed to occur via the dissociative adsorption of O_2 and low-temperature diffusion of lattice oxygen. Reduction of the CeO_2 support may also be promoted by the presence of Cu, as indicated by hydrogen spillover phenomena [9] and the formation of Ce^{3+} [10], which complicates attempts to attribute reactive oxygen species for the reaction to a particular site. Gamarra et al. [11] and independently by Polster et al. [12] reported a correlation between CO oxidation activity and the intensity of the DRIFTS carbonyl peak, which may suggest that the chemisorption of CO at Cu^+ or Cu^0 sites as an important stage of the overall reaction mechanism. In any case, the onset of catalytic activity often coincides with heightened levels of surface reducibility [13], suggesting the activity and selectivity of this catalytic formulation depend strongly on the redox properties of the catalyst. If it is accepted that carbonyl species are relevant to PROX as evident from infrared studies, it is not yet clear which species is really involved in the catalytic process, given a certain carbonyl speciation on the sample. It was within this framework that the following section of work was conducted.

Various synthetic procedures such as combustion [14], urea decomposition [15] and microemulsion [16] were employed in prior attempts to establish the nanostructural redox processes on the Cu–CeO_2 surface and relate these to the activity and mecha-

* Corresponding authors. Tel.: +41 44 823 4609 (D. Ferri), tel.: +852 3442 4627; fax: +852 2319 5927 (W.Y. Teoh).
E-mail addresses: davide.ferri@empa.ch (D. Ferri), wyteoh@cityu.edu.hk (W.Y. Teoh).
[1] Present address: School of Energy and Environment, City University of Hong Kong, Hong Kong Science Park, Shatin, N.T., Hong Kong.

0021-9517/$ - see front matter © 2010 Elsevier Inc. All rights reserved.
doi:10.1016/j.jcat.2010.10.009

nism of the catalyst. In the majority of the cases, different Cu–O morphologies, e.g. monomers, dimers [17], amorphous clusters [18] and crystallites, are produced, and it is difficult to accurately ascribe the specific structures to particular redox features. XANES study [11] found CO_2 selectivity loss occurring at similar temperatures to the formation of large concentrations of Cu^+ and Cu^0 and subsequently postulated that H_2 oxidation was occurring at the bulk copper oxide sites that were not adjacent to the ceria support, whereas CO oxidation was thought to be occurring specifically at interfacial sites between the two components. These findings suggested catalytic selectivity was determined by morphology, with different reaction sites for CO and H_2.

To better attribute the variations in catalytic selectivity to particular redox sites, the present work employs an active and well-defined catalyst, comprising exclusively of oxygen-bridged Cu dimers on ceria [17], prepared by flame spray pyrolysis (FSP) [19]. The homogeneity of the dimeric structure minimizes the complications associated with the coexistence of different copper oxide morphologies, allowing an exclusive focus on the redox mechanisms by which catalytic activity and selectivity were achieved. This will be conducted through a series of temperature-programmed studies coupled with *operando* diffuse reflectance infrared Fourier transform spectroscopy (DRIFTS) and modulation excitation spectroscopy (MES) [20].

2. Materials and methods

The 4% Cu–CeO_2 catalysts were synthesized using an FSP reactor [19,21], as detailed in our earlier publication [17]. Briefly, a precursor solution containing 0.5 M Ce was prepared by mixing cerium 2-ethylhexanoate (Strem, 49% solution in 2-ethylhexanoic acid) and Cu 2-ethylhexanoate (Aldrich, >99.9%) in xylene (Riedel de Haen, 96%). The liquid precursor was fed at a rate of 5 mL min^{-1} to the FSP nozzle by a syringe pump (Inotech R232) and dispersed with 5 L min^{-1} O_2 (1.5 bar, BOC Gases, >99.95%), forming fine spray droplets. Combustion of the spray droplets was instigated by a surrounding CH_4/O_2 (1.5 L min^{-1}/3.2 L min^{-1}, respectively) supporting flame, to form a primary core flame. An additional 5 L min^{-1} of sheath O_2 was issued through an outer sintered metal ring. The product particles were collected on a glass fibre filter (Whatmann GF/D) with the aid of a vacuum pump (Alcatel).

The catalytic activity of as-prepared catalysts was measured using 50 mg of the sample diluted with 75 mg α-alumina (sieve diameter 200–500 μm) in a packed bed reactor (I.D. 4 mm). A reactant gas mixture consisting of 0.5% CO, 2% O_2, 5% H_2 and balance He was employed at a flow rate of 60 mL min^{-1}. The bed temperature was increased in 10 °C increments over the 50–250 °C range. The composition of the effluent gas was determined by a Shimadzu GC-8 equipped with a Porapak column.

Temperature-programmed reduction (TPR) and desorption (TPD) experiments were performed on a Micromeritics Autochem 2920 equipped with a quadrupole mass spectrometer (MS, Balzers Thermostar, GSD 301T) operated in multiple-ion monitoring mode. Prior to both TPR and TPD, 100 mg of sample was pretreated at 300 °C under 50 mL min^{-1} of 5% O_2/He. TPR was performed under 5% H_2 or CO in He at 50 mL min^{-1} at a ramping rate of 5 °C min^{-1}. TPD was performed by flowing the probe gas (5% CO or H_2, balance He) under cooling to room temperature until the MS signal stabilized. The catalyst was then purged with 50 mL min^{-1} of Ar until background MS traces of the relevant mass fragments (H_2, CO, H_2O and CO_2) had returned to that of pure Ar (typically 1 h). The sample was heated under flowing Ar (50 mL min^{-1}) at a ramping rate of 5 °C min^{-1}.

Diffuse reflectance infrared (DRIFT) spectra were collected using a Vertex 70 infrared spectrometer (Bruker Optics) equipped with a DRIFT unit (Praying Mantis, Harrick) and a liquid nitrogen cooled MCT detector. The commercial Harrick cell (HVC-DRP-3), where the conventional dome was replaced by a flat CaF_2 window, was attached to a gas manifold system. Solenoid valves, electronically triggered using the rapid scan option of the OPUS software, were placed directly in front of the cell to minimize dead volume and allowed the rapid switch between gas flows. Gas exiting the cell was analysed online using a mass spectrometer (Pfeiffer, Omnistar). All spectra are reported in absorbance units and were corrected for the contribution of atmospheric CO_2 and water vapour only when needed. Prior to all experiments, the catalyst (ca. 60 mg) was calcined in situ at 400 °C for 1 h in a flow of 5% O_2/He (50 ml/min) and was cooled to room temperature. CO adsorption on Cu–CeO_2 was followed by admitting 1% CO/He (50 ml/min) for 45 min, after which either the flow was changed to He to follow desorption or the temperature was increased at 5 °C/min under CO/He up to 350 °C. A background spectrum was collected in He prior to admittance of CO. For the temperature-ramping experiment under PROX conditions, a spectrum was collected after calcination under the same atmosphere, which served as the background. Then, the 0.5% CO/5% H_2/4% O_2/He gas mixture was admitted to the cell (50 ml/min) and the contact with the catalyst was allowed for ca. 30 min. Finally, the temperature ramp was started by increasing the temperature in steps of 10 °C at 5 °C/min, and spectra were collected by co-adding 200 scans at 4 cm^{-1} resolution after the MS signals stabilized.

Concentration modulation experiments, see for example Ref. [22,23], in which the catalyst was contacted alternately with a flow of 0.5 vol.% CO/5 vol.% H_2/4 vol.% O_2 and 0.5 vol.% CO/5 vol.% H_2 (balance He; total flow, 50 ml/min) were performed at 80 °C and 140 °C. These temperatures corresponded to the low- and the high-activity regimes observed during the PROX ramp, respectively. The O_2 concentration was therefore varied between 0 and 4 vol.%, whereas the concentrations of CO and H_2 remained fixed. During a modulation period ($CO/H_2/O_2$ vs. CO/H_2; $T = 280$ s), twenty consecutive and equally long time-resolved spectra were collected by co-adding fifty interferograms at a scanner frequency of 80 kHz and a resolution of 4 cm^{-1}. Fifteen periods were performed at each temperature resulting in 300 time-resolved spectra. Each point spectrum of a period was averaged over the fifteen periods, and the resulting set of twenty spectra was processed into phase-resolved spectra using phase-sensitive detection (PSD) [20]. This procedure provides information on the correlation between signals (i.e. species), with enhanced signal-to-noise ratio with respect to the time-resolved spectra. It furthermore allows for filtering out all contributions of signals not responding with the same frequency as that of the stimulation (in this case, the O_2 concentration). In this way, weak signals can be separated from the contribution of more significant and overlapping signals, which appears to be especially required in the case of the CeO_2-containing samples.

3. Results and discussion

3.1. Catalytic preferential oxidation of carbon monoxide (CO-PROX)

A 4% Cu–CeO_2 sample (specific surface area = 93 m^2 g^{-1}) made by FSP [17,24] was selected as the working catalyst for identifying the CO-PROX mechanism. The physicochemical and structural properties of the catalyst were extensively characterized in our earlier publication [17]. Importantly, we identified the formation of surface-enriched dimeric CuO species on CeO_2, which was a key to the high activity and selectivity towards CO oxidation.

Under the PROX reaction conditions, i.e. in the presence of $CO/H_2/O_2$, two distinct operation regimes can be defined as shown in

Fig. 1. In Regime 1, at temperatures less than 150 °C, CO is selectively oxidized, with light-off occurring at <50 °C and no observed H_2 oxidation. At approximately 150 °C, there is a transition into Regime 2, where H_2 oxidation is initiated, resulting in a loss in catalytic selectivity. This process continues until complete consumption of the available O_2 supply at around 220 °C. Occurrence of the transition regime, which dictates the loss in selectivity, is of particular interest to this work. At this juncture, it is reasonable to anticipate a thermal-induced transformation in the characteristics of the catalyst structure. To investigate this effect, a series of temperature-programmed studies were developed to follow the characteristics of the redox reaction as a function of temperature.

3.2. Temperature-programmed studies

3.2.1. CO Temperature-programmed reduction (CO-TPR)

Fig. 2a depicts the CO and CO_2 concentrations downstream of the catalyst during CO-TPR, characterized by two peaks at 51 and 132 °C (α_1 and α_2, respectively). The low-temperature peak, α_1, coincides with the acceleration of catalytic activity seen at ~50 °C in Fig. 1. A mismatch between the temperatures of CO minima (58 °C) and CO_2 maxima (81 °C) could be attributed to the stabilization of intermediate carbonyl species and/or the high affinity of CO_2 to form various intermediate carbonates and formates on the catalyst and their subsequent low-temperature stability [25]. For the higher temperature reduction process, α_2, CO consumption and CO_2 evolution occur simultaneously at 132 °C, indicating further activation of a heterogeneous oxygen transfer mechanism and/or rapid decomposition of adsorbed species. In the latter case, adherence of various species on active sites may have limited the adsorption and reaction of incoming CO molecules. A prolonged tailing of CO consumption and CO_2 liberation exemplifies the case of hindered active sites, despite difficulties at this juncture in identifying whether the limitation stems from carbonate decomposition or lattice oxygen transfer.

It has been proposed in the literature that each TPR peak corresponds to a particular morphology that undergoes direct reduction from Cu^{2+} to Cu^0 [18,26] or represents the stage-wise reduction of CuO–Cu_2O and finally Cu^0 [9]. Here, the exclusive presence of oxygen-bridged CuO dimers in the current set of catalysts [17] discourages the notion of the former idea (to be confirmed by DRIFTS in a later section). The two distinct oxygen groups that can be removed by CO during the TPR process are tentatively assigned to the (1) removal of the bridging oxygen between the Cu atoms of the dimer (α_1, Eq. (1)), which have been previously demonstrated to be highly reducible [9], and (2) disruption of oxygen bonding between partially reduced Cu ions and the CeO_2 support to form metallic Cu atoms, Ce^{3+} ions [11] and an oxygen vacancy (α_2, Eq. (2)).

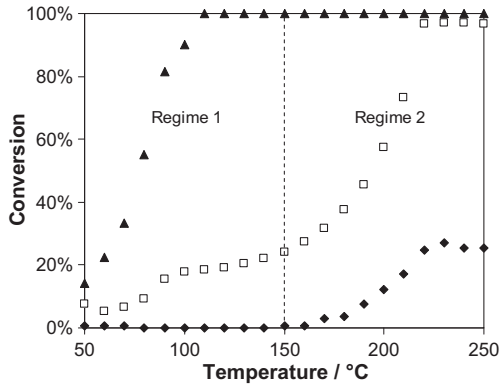

Fig. 1. Gas conversion profiles under PROX conditions. Catalyst: 4% Cu–CeO_2; reactant gas: (▲) CO; (□) O_2; (♦) H_2. Reactant gas: 0.5% CO, 2% O_2, 5% H_2, balance He; space velocity: 44,000 h^{-1}. Regime 1 shows the range of high catalytic selectivity towards CO oxidation, while in Regime 2 the selectivity is lost, i.e. oxidation of H_2.

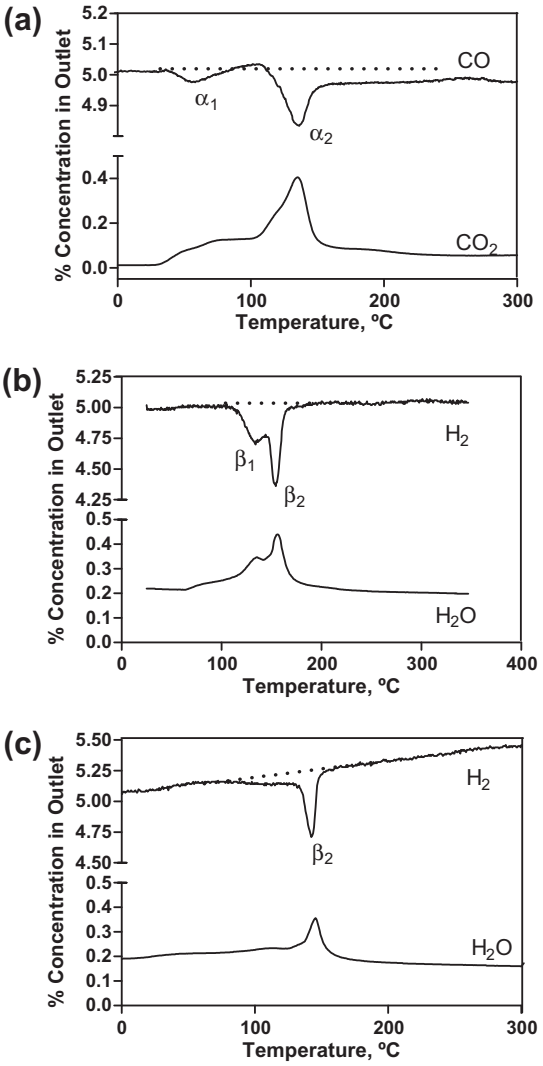

Fig. 2. Temperature-programmed reduction profile of 4 wt.% Cu–CeO_2 in (a) 5% CO/He, (b) 5% H_2/He and (c) 5% H_2/He following partial reduction by 5% CO/He to 70 °C. Shown are the traces of CO ($m/z = 28$), CO_2 ($m/z = 44$), H_2 ($m/z = 2$) and H_2O ($m/z = 18$). Temperature-ramping rates were 5 °C min^{-1} for all cases.

$$\alpha_1: \ \{Cu^{2+}\text{—}O^{2-}\text{—}Cu^{2+}\}^{2+} + CO \leftrightarrow 2Cu^{+} + CO_2 \quad (1)$$

$$\alpha_1: \ \{Cu^{+}\text{—}O^{2-}\text{—}Ce^{4+}\}^{3+} + CO \leftrightarrow Cu^{0} + Ce^{3+} + CO_2 \quad (2)$$

To further understand the interactions of the Cu–CeO_2 catalyst with another PROX reactant, H_2, a homologous H_2-TPR experiment was performed prior to combining sequential CO- and H_2-TPR. Splitting the two reactants is beneficial in untangling the competitive interactions between the two components.

3.2.2. H_2 Temperature-programmed reduction (H_2-TPR)

H_2-TPR of 4 wt.% Cu–CeO_2 (Fig. 2b) reveals two overlapping peaks, β_1 and β_2, centred at 129 and 151 °C, respectively. The moisture (H_2O) signal of β_1 corresponds directly to the consumption of H_2, implying a direct reduction of the catalyst surface, rather than chemisorption of H_2 as observed in Cu–CeO_2 catalysts prepared by other methods [27]. The broad shoulder on the low-temperature

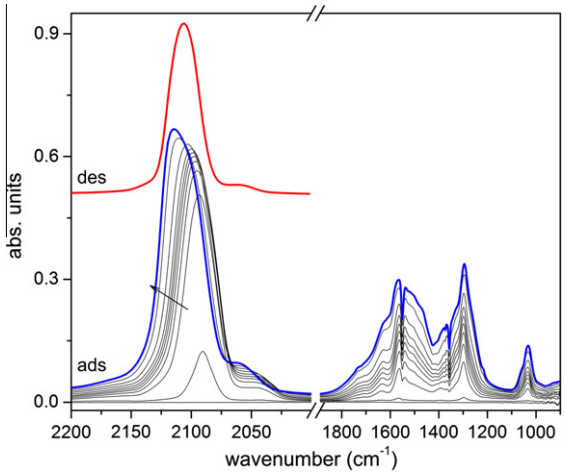

Fig. 3. DRIFTS spectra collected during CO adsorption at 25 °C on Cu–CeO_2. The blue spectrum is the final one measured prior to CO-TPR; the red spectrum (offset, for clarity) represents adsorbed CO resisting desorption with He (30 min) recorded in an independent CO adsorption–desorption experiment. The arrow indicates evolution of the major CO signal.

extreme of the H_2O peak (β_1) corresponds to the desorption of physisorbed moisture. As in the case of CO-TPR, H_2-TPR of Cu–CeO_2 proceeds via a CuO_x-like intermediate phase (where $x < 1$) [28], which rapidly converts to metallic Cu^0 particles in an oxygen deficient Ce^{3+}-containing lattice. Although the overlap of β_1 and β_2 peaks does not necessarily indicate the intermediate phase catalyses the secondary redox process, it does show the two processes occur with very similar activation energies.

Both CO- and H_2-TPR profiles contain two reduction events in the studied temperature range, however, the CO α_1 peak occurs at 50 °C lower than the H_2 β_1 peak. Comparison of the H_2-TPR and CO-TPR data (Section 3.2.3 and later using DRIFTS) provides supporting evidence that the α_1 reduction peak can be attributed to the formation of a partially reduced Cu^+ containing phase. As in the case of α_2, β_2 is likely to represent the reduction of this intermediate phase to form Cu^0, as well as an appreciable reduction of the CeO_2 support lattice to form Ce^{3+} via the provision of adjacent lattice oxygen [9,29]. If both of these processes correspond to the initial reduction stage of a redox mechanism, then the temperature difference is evidence of the thermodynamic and kinetic limitations of H_2, compared to CO.

3.2.3. Partial CO-TPR followed by H_2-TPR

To clarify whether there was any correlation between the two peaks detected in CO- and H_2-TPR, the α_1 stage of catalyst reduction was first completed (via partial reduction at 70 °C under 5% CO/He). The subsequently cooled and He-purged catalyst was then subjected to a standard H_2-TPR to obtain a TPR profile for the partially reduced intermediate CuO_x phase (Fig. 2c).

Whereas pure H_2-TPR resulted in two peaks (β_1 and β_2), following partial reduction in CO, the H_2 trace ($m/e = 2$) of the CuO_x intermediate phase displays only the single consumption event of the β_2 peak (Fig. 4). The absence of β_1 indicates a partial reduction of the catalyst by CO, which in turn disrupted or prevented the initial reaction, i.e. β_1, with H_2. A likely explanation is that the α_1 reduction under CO converted the majority of surface Cu^{2+}–Cu^+ [11], whereby there remained negligible species available for the β_1 transition. Importantly, Fig. 2c suggests that both H_2 and CO are capable of removing the same interfacial oxygen species via the respective β_1 and α_1 reactions and are most likely reacting at identical sites, despite CO doing so at lower temperatures. This may derive from a possible higher chemisorption affinity (i.e. carbonyl stabilization) of CO on Cu–CeO_2. The initial stabilization of carbonyl at reactive sites may in turn hinder the adsorption and oxidation of incoming H_2, thereby maintaining its high PROX selectivity below 150 °C.

At 150 °C and higher, the simultaneous occurrence of both α_2 and β_2 reduction processes results in the generation of Cu^0 species [11]. It is thought that such higher-order reduction of Cu sites enables CO to react rapidly with the surface without the need for stabilization at the reactive sites. In other words, CO and H_2 are now competing non-preferentially for the reactive sites, thereby losing the catalytic PROX selectivity. Under these non-selective conditions, while CO alone may be capable of generating some fraction of Cu^0 sites, the higher concentration of H_2 will further drive the redox equilibrium away from Cu^+ towards Cu^0. Dissociative adsorption of H_2 on metallic Cu can catalyse the spillover of atomic H onto the CeO_2 surface to form the Ce^{3+}–(OH)–Ce^{4+} type surface hydroxyls [30]. Via mutual condensation to form H_2O, these hydroxyls would increase the overall oxidation rate of H_2.

For further verification of the PROX mechanism, DRIFTS studies were undertaken, providing identification of the reaction sites responsible for CO oxidation. This provides new insights into the relationship between reaction mechanism and catalyst selectivity.

3.3. Diffuse reflectance infrared Fourier transform spectroscopy (DRIFTS)

3.3.1. CO Adsorption and TPR

Fig. 3 shows the spectra of adsorbed CO on CuO/CeO_2 at room temperature. Below 2000 cm^{-1}, signals attributable to the evolution of carbonates and formates were observed, which are due to the interaction of CO with CeO_2 [31]. These species were formed in addition to the already present carbonate-like and formate species on the catalyst surface (Fig. S1). Negative signals at 1550 and 1358 cm^{-1} coupled with the positive signals at 2933 and 2850 cm^{-1} (C–H stretch modes) reveal perturbation of the preexisting formates upon CO adsorption, most likely by rearrangement.

The signal of adsorbed CO evolves following extended exposure and is composed of low-, medium- and high-frequency components at ca. 2070–2050 cm^{-1}, 2110–2090 cm^{-1} and 2130–2115 cm^{-1}, respectively. The multiplicity of signals reveals a spontaneous variation in the extent of reduction of CuO/CeO_2 at room temperature, despite the well-defined character of the initial oxygen-bridged Cu dimers. For the Cu^{n+}–CO system, spectral ranges of 2200–2140 cm^{-1} and 2100–2000 cm^{-1} are typical for CO adsorption on Cu^{2+} and Cu^0 sites, respectively [32]. The former can be disregarded at room temperature (Fig. 3). The low-frequency feature at 2065 cm^{-1} is ascribed to CO adsorption at small metallic Cu clusters [33]. Attribution of the medium frequency peak is somewhat ambiguous according to the available literature. Vibrations in the vicinity of 2100–2090 cm^{-1} were previously ascribed to CO adsorption at 3D clusters of Cu^+–O–Cu^0 units supported on Al_2O_3 [33]; however, it has also been suggested that carbonyls formed upon Cu^+ atoms interacting strongly with the basic CeO_2 support will result in signals at a similar position [18]. The high-frequency feature at 2130–2110 cm^{-1} is considered to be due to CO adsorbed at Cu atoms directly bonded to adsorbed oxygen species [33].

The medium frequency signal (2090 cm^{-1}) is the first to appear in Fig. 3. It may result from the displacement of weakly adsorbed oxygen species at intrinsic Cu^+ defects at the surface [34]. The subsequent apparent blue-shift of the signal is likely due to spontaneous reduction of a fraction of the remaining Cu^{2+} component. Following equilibration, the spectrum is composed of an asymmetric signal centred at ca. 2115 cm^{-1} (Fig. 3, blue spectrum). The decrease in intensity and shift of the signal maximum to 2105 cm^{-1} when purging under He (red spectrum) is associated with the partial disappearance of the high- and low-frequency components.

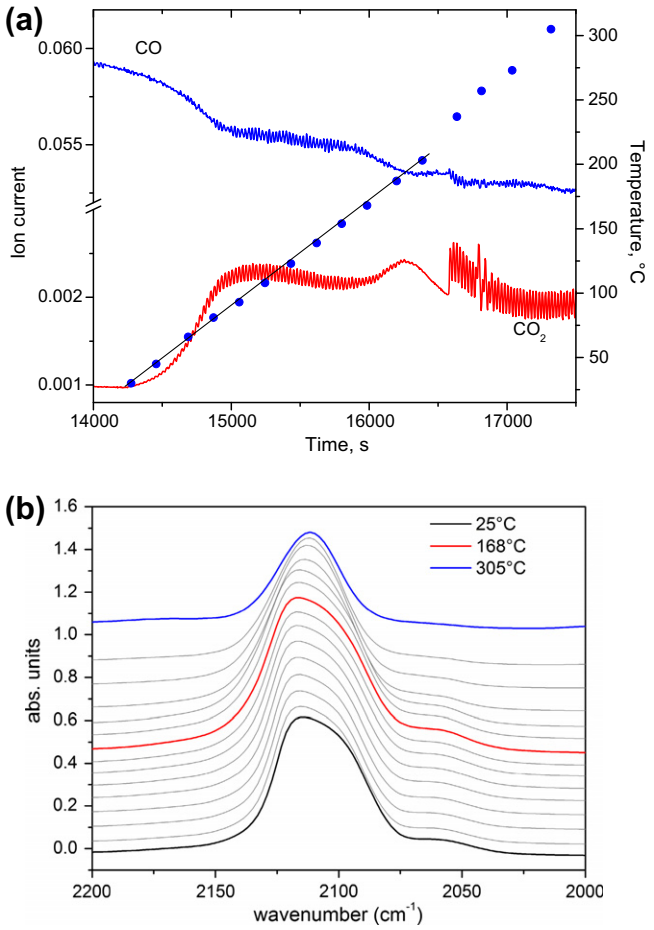

Fig. 4. (a) MS traces of signals CO (blue) and CO_2 (red) during CO-TPR on Cu–CeO_2 subsequent to CO adsorption at room temperature. (b) The carbonyl region of the DRIFT spectra recorded during the CO-TPR on Cu–CeO_2 in the temperature range 25–300 °C. Spectra are offset for clarity. (For interpretation of the references to colour in this figure legend, the reader is referred to the web version of this article.)

This instability can be taken as an indication of Cu^0–CO-related species, which tend to dissociate more readily under purging or evacuation [18,34]. The comparative stability of the medium frequency signal at ca. 2100 cm^{-1} suggests CO is adsorbed at Cu^+ centres on the surface of highly dispersed or disordered CuO [34]. Based on these assignments, the adsorption geometries are proposed in Scheme 1.

Fig. 4 shows the mass spectrometry (MS) traces and DRIFT spectra, recorded during CO-TPR after CO adsorption. In both cases, CO_2 desorption and CO consumption started from room temperature and at approximately 100 °C, there was a plateau in CO_2 desorption. In the low-temperature region between 25 and 80 °C, a slight blue-shift may reflect a greater extent of reduction than that occurring spontaneously at room temperature. Cu^+ ions are preferentially formed by this process, in agreement with the assignment of the α_1 peak in the CO-TPR results of Section 3.2.1. Beyond

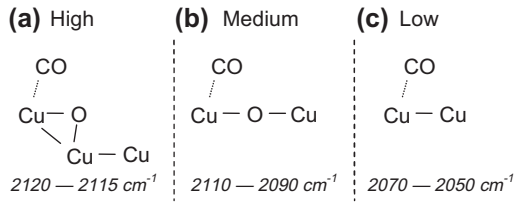

Scheme 1. Schematic depictions of adsorption geometries in the carbonyl region.

80 °C, the overall signal continues to grow on the high-energy side, further exaggerating the blue-shift and enduring until ca. 150 °C.

A second CO_2 desorption peak is observed at above 150 °C (Fig. 4a), accompanied by gradual attenuation of the carbonyl signal and its red-shift to 2111 cm^{-1}. The carbonyl peak position becomes constant at above 210 °C. The red-shift is consistent with the α_2 reduction, which yields Cu^0–CO. More interestingly, the attenuated signal shows the decreased effect of carbonyl stabilization due to the weaker bonding between Cu^0 and CO [18,34]. Attenuation of the carbonyl signal above 210 °C is associated with an overall increase in the population of various carbonate and formate species (Fig. S2), suggesting that the residence time of CO (and associated intermediates) on CeO_2 increases with temperature and the desorption of carbonate and formate species is a slower step.

3.3.2. Preferential oxidation (PROX)

Fig. 5 depicts the changes that occur in the carbonyl region when Cu–CeO_2 is contacted with the PROX mixture ($CO/H_2/O_2$) at room temperature and then subjected to temperature ramping. The inset shows a magnification of the gas-phase CO_2 region over the same temperature range. At room temperature, an initial signal at ca. 2095 cm^{-1} is observed to gradually convert into an asymmetric carbonyl signal with a maximum at ca. 2110 cm^{-1}. The earlier peak assignments determined for CO adsorption and CO-TPR suggest the CO adsorbs primarily at several different Cu^+ sites, with a minor population of metallic Cu^0–CO carbonyls.

The MS data (Fig. 6) demonstrate low levels of activity in the DRIFTS cell are present at 40–50 °C, with light-off occurring around 70 °C and maximum activity attained at 140–150 °C. The slight differences between this trend and the catalytic activity findings (Section 3.1) are most likely due to differences in reactor geometry. The increase in CO_2 production over this temperature range is reflected in intensification of the gas-phase CO_2 peak (2345 cm^{-1}) in the inset of Fig. 5. At higher temperatures, the concentration of water

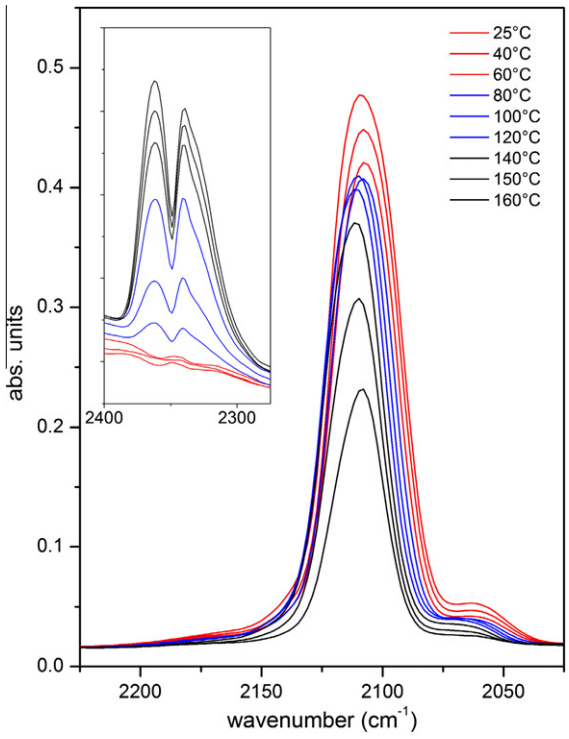

Fig. 5. DRIFTS spectra during PROX reaction on Cu–CeO_2. The carbonyl region (2050–2150 cm^{-1}) is shown. Inset: Magnification of the gas-phase CO_2 region.

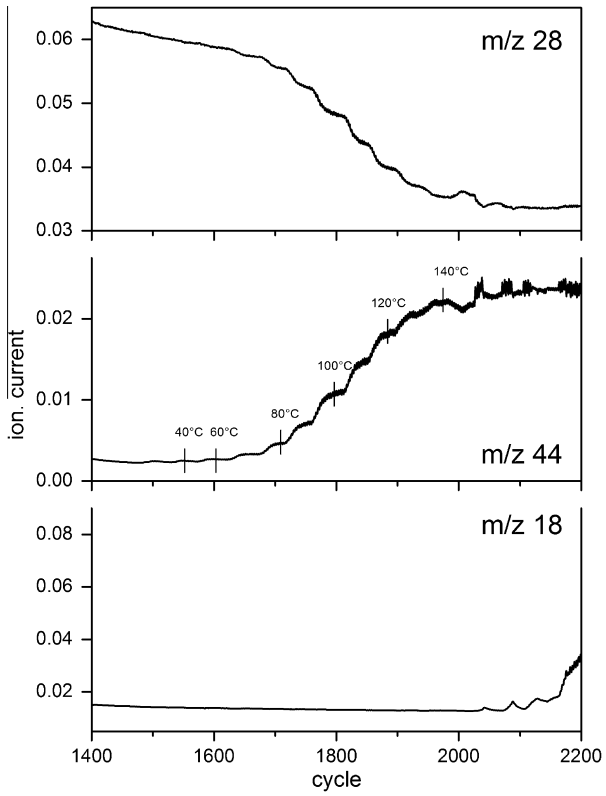

Fig. 6. MS traces of signals corresponding to CO ($m/z = 28$), CO_2 ($m/z = 44$) and H_2O ($m/z = 18$) during PROX reaction on Cu–CeO_2.

from catalytic H_2 oxidation increases, agreeing with earlier PROX activity and selectivity findings (Fig. 1).

The intensity and position of the carbonyl peak undergoes a series of changes with increasing reaction temperature (Fig. 5). Comparing the peak maxima from 40 to 80 °C, a decrease in overall intensity is apparent. The lack of H_2O production observed at this temperature range confirms H_2 is not interacting with the surface. At 80–140 °C, the carbonyl signal undergoes a blue-shift, likely caused by the α_1 reduction process detected by CO-TPR. This redox reaction populates the surface with a mixture of Cu^+ and Cu^0, which, when bonded via a surface oxygen, produces the higher frequency mode proposed in Scheme 1. Dissociation of chemisorbed O species could also generate a blue-shift by weakening the Cu–CO bond [35]. Importantly, although the carbonyl IR intensity decreases slightly, the gas-phase CO_2 intensity (detected by DRIFTS and MS) increases considerably, agreeing with the region of high PROX activity and selectivity. That is, there exists a region of carbonyl stabilization (i.e. a slow step) on the oxidation sites that possibly prevented the adsorption of any incoming H_2, in turn preserving its high catalytic selectivity. Recalling the prior discussion on TPR findings, it is possible CO and H_2 oxidation share identical active sites.

At 150 °C and beyond, the carbonyl signal undergoes a monotonic red-shift and intensity loss. The low-energy shift implies a reduction of surface Cu to the metallic state, via the consumption of Cu^+ sites. Despite the decrease in carbonyl intensity, CO_2 signals (from DRIFTS and MS) only increase slightly. Moreover, it is evident from MS that H_2 oxidation commences at above 150 °C. These findings, along with the H_2-TPR profile (Fig. 2b) demonstrating the β_1 and β_2 redox reactions occur in this region, provide further evidence the loss of catalytic selectivity is due to the redox reaction between Cu^+ and H_2 to produce metallic Cu and H_2O. Taken together, they infer the loss in carbonyl stabilization as a result of significant reduction to Cu^0 allows competitive adsorption between incoming CO and H_2 for active sites, and thereby providing a plausible explanation for the loss in PROX selectivity.

Analysis of the region below 2000 cm^{-1} (not shown), where various carbonates and formate species are identifiable, could not at this stage provide conclusive information on the involvement of these adsorbates in the surface processes. This effect most likely derived from the strong intensity of the complex envelope entailing all species predominantly populating the CeO_2 support. More detailed surface studies with regard to the role of carbonates and formates are still required in relevance to the CO_2 evolution and desorption.

3.3.3. Transient studies

The conventional representation of time-resolved DRIFT spectra under steady state conditions (as in Sections 3.3.1 and 3.3.2) is inadequate to differentiate between species involved in the catalytic event and spectator species. For example, while a strong carbonyl signal was detected under reaction conditions (Fig. 5), there was no direct evidence of the species (Scheme 1) participating in the oxidation reaction. To circumvent this problem and to further confirm the PROX mechanistic, Cu–CeO_2 was repeatedly submitted to transients in oxygen concentration (oxygen concentration modulation). Oxygen was 'pulsed' into a continuous CO/H_2 mixture at the concentrations used in the PROX experiment to generate a set of time-resolved spectra at 80 and 140 °C, i.e. the two edges of the selectivity window.

The MS data recorded during the O_2 pulses at 140 °C (Fig. 7) reveal enhanced CO_2 production a few seconds after O_2 is supplied to the catalyst. Catalytic activity is relatively stable in the presence of O_2, but drops following conclusion of the pulse. The periodic fluctuation in H_2O and H_2 signals also indicates low levels of H_2 oxida-

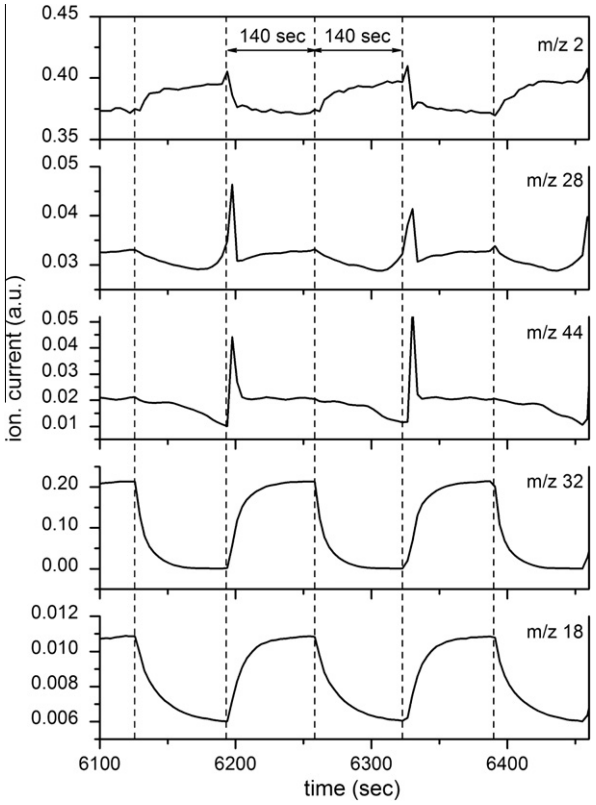

Fig. 7. MS traces of H_2 ($m/z = 2$), O_2 ($m/z = 32$), CO ($m/z = 28$), CO_2 ($m/z = 44$) and H_2O ($m/z = 18$) as a function of time during O_2 pulse cycles: $CO/H_2/O_2$ vs. CO/H_2 on Cu–CeO_2 at 140 °C. Vertical dash lines represent the size of half-periods (140 s).

tion at 140 °C. At 80 °C (not shown), no CO_2 production peak was observed, which is associated with the low level of activity at that temperature (Fig. 6).

Fig. 8a depicts two selected time-resolved spectra corresponding to the maximum variation in carbonyl signal intensity. No appreciable changes can be observed in the region below 2000 cm^{-1}. The time-resolved spectra were converted into phase-resolved spectra by PSD (Fig. 8b) [20]. In addition to the changes observed for the carbonyl species, the phase-resolved spectra provide information on weak variations associated with carbonate and formate species with enhanced signal-to-noise ratio. Despite this being the case, it remains difficult to associate unambiguously, at least at this stage, the role of these species with a specific reaction mechanism.

The phase-resolved spectra at 140 °C are dominated by two signals at 2120 and 2099 cm^{-1}. The two carbonyl signals are anti-correlated with respect to the CO_2 signal (2361 cm^{-1}), i.e. carbonyl minima approximately coincide with gas-phase CO_2 formation maxima. This is evidence of the two carbonyl species being directly involved in the oxidation mechanism and potentially corresponding to two different active species. Comparing the time- and phase-resolved (Fig. 8) spectra in the carbonyl region indicates the intensity change associated with the CO signals corresponds to periodic formation and consumption of CO species during a full $CO/O_2/H_2$–CO/H_2 modulation period. However, these changes occur on top of a constant surface carbonyl concentration.

Fig. 9 shows in detail the phase-resolved spectra obtained at 80 and 140 °C in the carbonyl region. Overall, the changes in the carbonyl signal are more pronounced at 140 °C, as it would be expected from the decreased carbonyl stabilization at high temperatures as well as the higher rate of CO_2 production. At 80 °C, the signal at 2099 cm^{-1} undergoes the largest intensity change following the O_2 pulse. Based on our previous assignment,

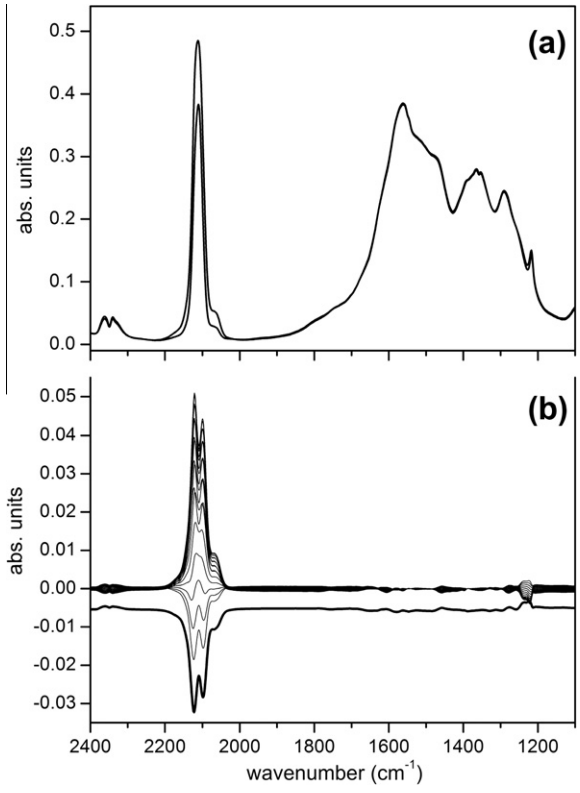

Fig. 8. (a) Time- and (b) phase-resolved spectra during oxygen concentration modulation: $CO/H_2/O_2$ vs. CO/H_2 on Cu–CeO_2 at 140 °C. A phase-resolved spectrum is offset to show the anti-correlation of gas-phase CO_2 and carbonyl species.

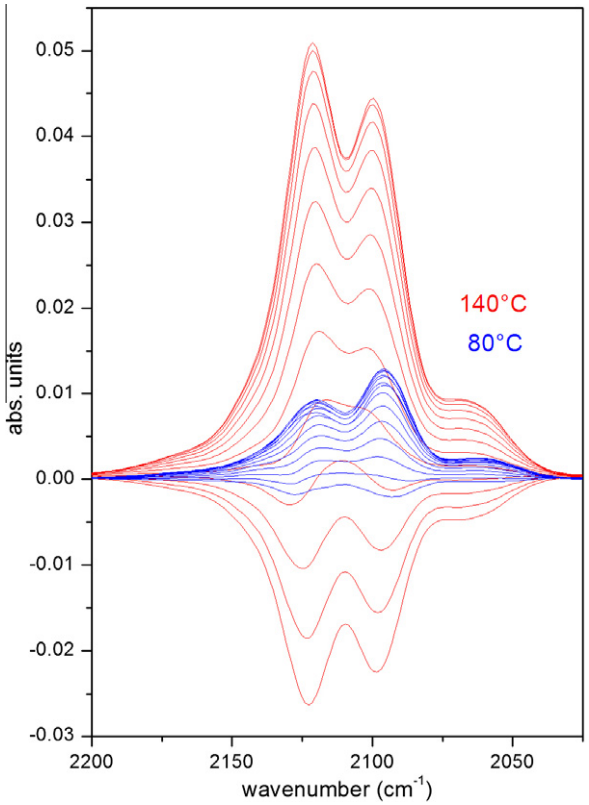

Fig. 9. Comparison of the carbonyl region of phase-resolved spectra during oxygen modulation: $CO/H_2/O_2$ vs. CO/H_2 on Cu–CeO_2 at 80 and 140 °C.

this signal is a likely result from CO adsorbed on coordinately unsaturated Cu^+ sites (Scheme 1b). The feature at 2120 cm^{-1} is tentatively ascribed to CO adsorbed at partially oxidized Cu sites, which are also bonded to adjacent metallic Cu^0 (Scheme 1c). This species is anticipated as the one providing the blue-shift in the overall carbonyl signal observed in Fig. 5. Importantly, it is evident from Fig. 9 that the two carbonyl signals respond differently to the temperature increase. The signal at 2120 cm^{-1} undergoes a greater intensity change at 140 °C than at 80 °C and is therefore more temperature sensitive. Furthermore, it is associated with a species (Scheme 1c) that is more sensitive to the external stimulation (oxygen concentration modulation) and hence is more involved in CO oxidation than the structure of Scheme 1b. Gradual reduction of the catalyst surface at high temperatures, particularly following the onset of H_2 oxidation, naturally increases the population of higher frequency carbonyls (Scheme 1c). The minor component at 2060 cm^{-1} (Scheme 1a) also experiences some temperature-induced amplification, which is expected given the increased concentration of metallic Cu clusters at higher temperature.

4. Conclusions

In this work, flame-prepared 4 wt.% Cu–CeO_2 catalysts, comprising Cu dimers supported on a CeO_2 lattice, were tested for the preferential oxidation of CO (in excess H_2). Performance of the catalyst could be separated into selective and non-selective regimes at low (<150 °C) and high (⩾150 °C) temperatures, respectively. The light-off in catalytic activity corresponded to initial CO-induced surface reduction, where surface divalent Cu was converted to monovalent species. Combined TPR and DRIFTS studies suggested a preferential carbonyl stabilization effect (i.e. Cu^+–CO) at below 150 °C, which prevented the adsorption and oxidation

of H_2 on otherwise identical reaction sites. Further reduction to metallic Cu at above 150 °C prompted a loss in carbonyl stabilization. As a result, CO and H_2 were competing for the adsorption on oxidation sites, promoting a loss in selectivity, manifested as simultaneous CO and H_2 oxidation. Changes in the phase-angle delay between carbonyl signal diminution and CO_2 evolution during concentration modulation DRIFTS experiments suggested the simultaneous oxidation of H_2 may retard the CO_2 evolution rate at high temperatures.

Acknowledgements

The authors thank the Australian Research Council (ARC) for financial support through the ARC Centre of Excellence for Functional Nanomaterials. D.F. thanks Empa for financial support.

Appendix A. Supplementary material

Supplementary data associated with this article can be found, in the online version, at doi:10.1016/j.jcat.2010.10.009.

References

[1] J. Park, X.G. Li, J. Power Sources 163 (2007) 853.
[2] D.L. Trimm, Z.I. Onsan, Catal. Rev. 43 (2001) 31.
[3] G. Avgouropoulos, T. Ioannides, Ch. Papadopoulou, J. Batista, S. Hocevar, H.K. Matralis, Catal. Today 75 (2002) 157.
[4] G. Sedmak, S. Hocevar, J. Levec, J. Catal. 213 (2003) 135.
[5] Y. Liu, Q. Fu, M. Flytzani-Stephanopoulos, Catal. Today 93–95 (2004) 241.
[6] G. Marban, A.B. Fuertes, Appl. Catal. B 57 (2005) 43.
[7] C.M. Bae, J.B. Ko, D.H. Kim, Catal. Commun. 6 (2005) 507.
[8] G. Sedmak, S. Hocevar, J. Levec, J. Catal. 222 (2004) 87.
[9] A. Tschope, M.L. Trudeau, J.Y. Ying, J. Phys. Chem. B 103 (1999) 8858.
[10] X. Tang, B. Zhang, Y. Li, Y. Xu, Q. Xin, W. Shen, Appl. Catal. A 288 (2005) 116.
[11] D. Gamarra, C. Belver, M. Fernandez-Garcia, A. Martinez-Arias, J. Am. Chem. Soc. 129 (2007) 12064.
[12] C.S. Polster, H. Nair, C.D. Baertsch, J. Catal. 266 (2009) 308.
[13] M.-F. Luo, Y.-J. Zhong, X.-X. Yuan, X.-M. Zheng, Appl. Catal. A 162 (1997) 121.
[14] G.R. Rao, H.R. Sahu, B.G. Mishra, Colloids Surf. A 220 (2003) 261.
[15] G. Avgouropoulos, T. Ioannides, H. Matralis, Appl. Catal. B 56 (2005) 87.
[16] X.Q. Wang, J.A. Rodriguez, J.C. Hanson, D. Gamarra, A. Martinez-Arias, M. Fernandez-Garcia, J. Phys. Chem. B 109 (2005) 19595.
[17] R. Kydd, W.Y. Teoh, K. Wong, Y. Wang, J. Scott, Q.H. Zeng, A.B. Yu, J. Zou, R. Amal, Adv. Funct. Mater. 19 (2009) 369.
[18] A. Martinez-Arias, M. Fernandez-Garcia, J. Soria, J.C. Conesa, J. Catal. 182 (1999) 367.
[19] W.Y. Teoh, L. Mädler, R. Amal, Nanoscale 2 (2010) 1324.
[20] D. Baurecht, U.P. Fringeli, Rev. Sci. Instrum. 72 (2001) 3782.
[21] W.Y. Teoh, L. Mädler, D. Beydoun, S.E. Pratsinis, R. Amal, Chem. Eng. Sci. 60 (2005) 5852.
[22] T. Bürgi, A. Baiker, J. Phys. Chem. B 106 (2002) 10649.
[23] A. Urakawa, T. Bürgi, H.-P. Schläpfer, A. Baiker, J. Chem. Phys. 124 (2006) 54717.
[24] R. Kydd, W.Y. Teoh, J. Scott, D. Ferri, R. Amal, ChemCatChem 1 (2009) 286.
[25] T. Caputo, L. Lisi, R. Pirone, G. Russo, Appl. Catal. A 348 (2008) 42.
[26] D. Gamarra, A. Hornes, Z. Koppany, Z. Schay, G. Munuera, J. Soria, A. Martinez-Arias, J. Power Sources 169 (2007) 110.
[27] Q. Wang, J.C. Hanson, A.I. Frenkel, J. Chem. Phys. 129 (2008) 234502.
[28] D. Gamarra, G. Munuera, A.B. Hungria, M. Fernandez-Garcia, J.C. Conesa, P.A. Midgley, X.Q. Wang, J.C. Hanson, J.A. Rodriguez, A. Martinez-Arias, J. Phys. Chem. C 111 (2007) 11026.
[29] A. Martinez-Arias, M. Fernandez-Garcia, O. Galvez, J.M. Coronado, J.A. Anderson, J.C. Conesa, J. Soria, G. Munuera, J. Catal. 195 (2000) 207.
[30] K.A. Pokrovski, A.T. Bell, J. Catal. 241 (2006) 276.
[31] O. Pozdnyakova, D. Teschner, A. Wootsch, J. Kröhnert, B. Steinhauer, H. Sauer, L. Toth, F.C. Jentoft, A. Knop-Gericke, Z. Paal, R. Schlögl, J. Catal. 237 (2006) 17.
[32] M. Manzoli, R. Di Monte, F. Boccuzzi, S. Coluccia, J. Kaspar, Appl. Catal. B 61 (2005) 192.
[33] F. Boccuzzi, G. Ghiotti, A. Chiorino, Surf. Sci. 162 (1985) 361.
[34] S.F. Tikhov, V.A. Sadykov, G.N. Kryukova, E.A. Paukshtis, V.V. Popovskii, T.G. Starostina, G.V. Kharlamov, V.F. Anufrienko, V.F. Poluboyarov, V.A. Razdobarov, N.N. Bulgakov, A.V. Kalinkin, J. Catal. 134 (1992) 506.
[35] C.M. Kim, C.-W. Yi, D.W. Goodman, J. Phys. Chem. B 109 (2005) 1891.